HAL
open science

Influence of macromixing on powder formation in a reactive coaxial jet

Carine Ablitzer-Thouroude, Frédéric Gruy, Christophe Perrais

To cite this version:

Carine Ablitzer-Thouroude, Frédéric Gruy, Christophe Perrais. Influence of macromixing on powder formation in a reactive coaxial jet. Chemical Engineering Science, 2002, 57 (14), pp.2837-2848. 10.1016/S0009-2509(02)00148-3 . emse-03760552

HAL Id: emse-03760552

https://hal-emse.ccsd.cnrs.fr/emse-03760552v1

Submitted on 25 Aug 2022

HAL is a multi-disciplinary open access archive for the deposit and dissemination of scientific research documents, whether they are published or not. The documents may come from teaching and research institutions in France or abroad, or from public or private research centers.

L'archive ouverte pluridisciplinaire **HAL**, est destinée au dépôt et à la diffusion de documents scientifiques de niveau recherche, publiés ou non, émanant des établissements d'enseignement et de recherche français ou étrangers, des laboratoires publics ou privés.

Influence of macromixing on powder formation in a reactive coaxial jet

C. Ablitzer* [(1)], F. Gruy[(2)] and C. Perrais[(1)]

[(1)] *CEA, Centre d'Etudes de Cadarache, DEN/CAD/DEC/SPUA/LCU, 13108 Saint-Paul Lez Durance Cedex, France*
[(2)] *Ecole Nationale Supérieure des Mines de Saint-Etienne, 158 Cours Fauriel, 42023 Saint-Etienne Cedex 2, France*

* *Corresponding author*

Abstract

This paper deals with an experimental study and a modelling of the formation of particles in a reactive gaseous jet. Particles result from the gas-phase hydrolysis of tin tetrachloride in a turbulent coaxial jet. In presented experiments, the influence of velocities of gases and nozzle shape on particle size distributions has been studied. Experimental distributions have been evaluated by in situ light-scattering measurements. Theoretical particle size distributions resulting from a simple model are compared to experimental measurements. Results show that particles do not seem to grow only by agglomeration and mixing near the nozzle may strongly influence final particle size distributions. In fact, the development of mixing layers near the nozzle appears to have little effect on particle size distributions, so that mesomixing could be the major phenomenon.

Keywords : coaxial jets, precipitation, mixing, agglomeration, gases, particle formation

---

1. Introduction

Particles can be produced in reactive turbulent coaxial jets. This kind of jet has mostly been studied from a flow-field point of view, in inert coaxial jets with gases of identical densities. The influence of velocities ratio has been particularly investigated because macromixing mostly results from shear phenomena for these systems. The effects of nozzle shape and confinement have also been punctually evaluated (Buresti, Talamelli & Petagna,

1994 ; Buresti, Petagna & Talamelli, 1998 ; Habib & Whitelaw, 1979 ; Champagne & Wygnanski, 1971).

Two or three zones are often distinguished in coaxial jets. The initial region of the jet corresponds to the development of mixing layers between gases : an inner mixing layer between the inner gas and the outer gas, and an outer mixing layer between the outer gas and the atmospheric gas (Ko & Kwan, 1976). Far from the nozzle (several tens inner diameters away), the structure of the double jet is the same as that of a simple jet. This region, characterised by self-similar profiles for velocities and density, is the principal region -or similarity region- of the jet. Self-similar profiles for velocities and density have also been reported for shear mixing layers. The transition zone between initial and principal regions has been little studied.

Self-similarity of velocities has been studied by several authors. Champagne & Wygnanski (1971) and Durao & Withelaw (1973) were particularly interested in the characteristics of the principal region. Ko & Kwan (1976), Ko & Au (1985), Buresti et al. (1994, 1998) and Au & Ko (1987) also studied the near-field of coaxial jets. Habib & Whitelaw (1979) have more particularly considered the influence of confinement.

The visualisation of vortex structures in coaxial jets has also been performed. For example, Dahm, Frieler & Tryggvason (1992) visualised the development of vortices for various sets of velocities. They obtained several vortex patterns depending on both absolute and relative velocities. More recently, Favre-Marinet, Camano & Sarboch (1999) have studied coaxial jets of gases with large density differences ; they have observed a recirculation regime for large velocity ratios.

Formation of particles in gases in general has been reviewed by Pratsinis & Vemury (1996). Particle formation in jets is common in that kind of processes. Characteristics of

particles are then often of interest. To this end, Lesniewski (1997) has recently studied several kinds of reactive simple jets. He distinguished nucleation-controlled jets and coagulation-controlled jets, as a function of initial supersaturation. Particle size distributions (PSD) in the jet seem to depend highly on the controlling phenomenon. Evaluations of PSD as a function of axial distance are proposed by Lesniewski for each case. For coagulation-controlled jets, he uses results of studies of Delattre & Friedlander (1978) and Koch, Windt & Karfich (1993). They deal with coagulation in the free molecule regime and in the continuum regime.

In this work, an experimental study and a modelling of particle formation in tin tetrachloride ($SnCl_4$)/water vapour (H_2O) coaxial jets have been undertaken in order to control PSD better, as a function of operating conditions. In a previous paper (Ablitzer, Gruy & Perrais, 2001), PSD from $TiCl_4/H_2O$ and $SnCl_4/H_2O$ jets, obtained with various sets of velocities, have been compared. For $TiCl_4/H_2O$ double concentric jets, mean diameters remain nearly unchanged in the range of our experiments. On the contrary, for $SnCl_4/H_2O$ double concentric jets, mean diameters seem to be strongly influenced by exit velocities. A simple model with no adjustable parameter has been built in order to describe mixing of gases, as well as nucleation and growth of particles in a reactive coaxial jet. A comparison of theoretical and experimental results shows that particles obtained by hydrolysis of $TiCl_4$ in a double coaxial jet seem to grow mainly through agglomeration, in agreement with the proposed model, whereas another growth phenomenon may be involved for particles obtained by hydrolysis of $SnCl_4$.

Additional studies have been performed with the $SnCl_4/H_2O$ system in order to identify relevant phenomena. The influence of various parameters has been studied, especially velocities of gases, densities of gases and nozzle shape.

A description of the experimental apparatus is given in section 2, with the set-up for reactive and non reactive jets production and the probe for in situ light-scattering measurements.

Section 3 is devoted to an experimental and theoretical study of the development of mixing layers in a double coaxial jet for gases of various densities. Section 4 presents experimental PSD obtained with reactive $SnCl_4/H_2O$ coaxial jets. A modelling of reactive jets is discussed in section 5.

2. Experimental set-up

2.1. Apparatus

The experimental set-up can be used for the production and study of non reactive or reactive jets. Our experimental jets are considered to be turbulent jets.

The experimental apparatus for reactive jets is described in a previous paper (Ablitzer et al., 2001). It consists of two cylinders with pistons connected to a nozzle (Fig. 1). Cylinders are previously filled with diluted gaseous tin tetrachloride (inner gas, index 1) and water vapour (outer gas, index 2). The reactive jet results from a single and simultaneous push down of the two pistons. It is vertical and develops downwards, in stagnant air at room temperature. It ends automatically when one of the two cylinders is empty, so that durations between 5 s and 34 s are obtained. Partial pressures of tin tetrachloride and water vapour are moderate ; they range from 3.5 kPa (± 0.5 kPa) to 10.0 kPa (± 0.5 kPa). Partial pressures of 7.1 kPa (± 0.5 kPa) have been generally used. Nitrogen was the carrier gas for both reagents for most experiments but several have also been performed with two gases with strongly different densities : helium and argon. Reactive gases are heated to 300°C before they enter the nozzle. Before the beginning of the jet, nozzle and connected tubes are heated with air or nitrogen coming from a bypass. Exit velocities (W_1, W_2) range from 10 to 100 $m.s^{-1}$. Velocities can be set independently one from the other.

For non reactive jets, pistons can be by-passed in order to perform continuous experiments with various inert gases (air, argon or helium). Velocities are then regulated with

volumetric flow-meters. Inner and outer velocities generally ranged from 20 $m.s^{-1}$ to 50 $m.s^{-1}$. For air/air jets, these values correspond to Reynolds numbers ranging from about 4000 to 10000 for both inner and outer jets. For argon/helium jets, these values correspond to Reynolds numbers ranging from about 4000 to 10000 for inner jet and from about 500 to 1200 for outer jet.

2.2. Nozzles

Four different axisymmetric nozzles have been used in our experiments : two for double jets and two for triple jets. They have been shaped with concentric tubes made of stainless steel. Their characteristics are described in Tab. 1.

For each type of nozzle (double and triple), tubes with a thickness of 0.2 mm or 1.0 mm have been used in order to study the influence of this parameter on resulting PSD. The use of triple coaxial nozzles makes it possible to evaluate the influence of an intermediate flow of inert gas (nitrogen).

2.3. Temperature measurements

Macromixing of reagents has been studied through temperature measurements in non reactive jets. We used inert gases having equal densities (air/air) or very different densities (helium/argon), the heavier gas corresponding then to the inner jet. If the outer gas is hotter than the inner one, the end of the secondary core (area where the outer gas is still pure) corresponds to a sudden decrease of the maximal temperature in planes perpendicular to the axis, as a function of the axial distance (Fig. 2). The same kind of measurements could be performed for the length of the primary core, with the inner gas hotter than the outer one.

The probe used for measurements is a 125 µm in diameter chromel-alumel thermocouple.

2.4. Particle sizing

A photograph of particles obtained is shown in Fig. 3. Particles are spherical so that coalescence of agglomerates is total. Diameters range from 0.1 to 1.0 µm.

Experimental PSD have been obtained by in situ light-scattering measurements. White light was supplied by a high-pressure Xe-Hg arc lamp Hamamatsu 75 W. It was carried to the probe with an optical fibre (200 µm in diameter). Convergent lenses ensured the beam collimation in the measurement zone. The turbidimetric probe had a 7.4 cm optical path (L) and was flushed with nitrogen in order to avoid depositions on the lenses (Fig. 4). The transmitted light was again carried with an optical fibre to a 300-1100 nm spectrometer MMS visible DLK and analysed. The probe was in a plane perpendicular to the jet axis and crossed the axis 3 cm away from the exit of the nozzle.

If $I_0(\lambda)$ is the light intensity without any particle and $I(\lambda)$ the light intensity with particles, the turbidity for each wavelength λ is defined as follows (Eq. 1) :

$$\tau_{(\lambda)} = \frac{1}{L}\ln\left(\frac{I_{0(\lambda)}}{I_{(\lambda)}}\right) \qquad (1)$$

The turbidity of a polydisperse suspension of spheres is linked to the particle size distribution by the Mie theory (Saint-Raymond, Gruy & Cournil, 1998).

PSD in the container are assumed to be log-normal, so that the determination of an experimental distribution consists in determining the mean diameter and the relative standard deviation that best fit the turbidity curve. A micrograph analysis (from SEM observations) is in agreement with the assumption of a monomodal distribution.

No reliable measurement has been done inside the jet. Indeed, the optical path length of the probe is large (7.4 cm) so that particles inside and outside the jet may coexist in the measurement zone. Besides, particles in the jet are often too small to be measured. So axial and radial variations of PSD in the jet have not been measured. However reliable measurements have been obtained on the first particles having reached the end of the jet and passing again through the probe because of convection, about 6 seconds after they left the jet (see Fig. 1). Global measurements have also been made in the homogeneous suspension of particles in the container, 15 seconds after the end of the jet. Distributions of so called "firstly measured particles" (PSD1) are supposed to be only slightly affected by the way particles disperse in the container after the jet whereas distributions of so called "particles 15s after the end of the jet" (PSD2) are strongly dependent on jet duration and characteristics of agglomeration in the container. However, measurements are more accurate for particles 15s after the end of the jet because particles are bigger and a longer measurement time can be used.

From our measurements and with the hypothesis of log-normal PSD, distributions in the container appear to have a relative standard deviation always close to 0.3. As a result, in this paper comparisons of PSD will only consist in comparisons of mean diameters.

3. Influence of densities on macromixing

Densities of gases are known to have an influence on the development of turbulent mixing layers (Brown & Roshko, 1974 ; Dimotakis, 1986 ; Favre-Marinet et al., 1999). So, this point has been taken into account for the theoretical description of macromixing in the jet and temperature measurements have been made on inert jets with gases of various densities.

3.1. Modelling

Abramovich (1963) has proposed a phenomenological description of the development of shear mixing layers (Eq. 2) :

$$\frac{d\delta}{dz}=c_\delta \frac{W_1-W_2}{W_c} \tag{2}$$

where δ is a finite thickness characterising the mixing layer and W_c a characteristic velocity linked to the profiles of axial velocity and density (Eq. 3) :

$$W_c(z)=\frac{\int_{layer}\rho(r,z)w(r,z)dr}{\int_{layer}\rho(r,z)dr} \tag{3}$$

where r and z are radial and axial distances in cylindrical co-ordinates.

These profiles are commonly supposed to be self-similar. c_δ is a constant close to 0.135.

Viswanathan & Morris (1992) have proposed a more theoretical approach based on local conservation equations of mass and momentum for a turbulent shear-layer. The components of velocity (u,v,w) in cylindrical co-ordinates (r,θ,z) consist of a mean term ($\overline{u},\overline{v},\overline{w}$) and a fluctuating one (u',v',w'). After several simplifications, the conservation equations for a stationary system become (Eq. 4 and Eq. 5) :

$$\frac{1}{r}\frac{\partial(\overline{\rho ur})}{\partial r}+\frac{\partial(\overline{\rho w})}{\partial z}=0 \tag{4}$$

$$\overline{\rho u}\frac{\partial\overline{w}}{\partial r}+\overline{\rho w}\frac{\partial\overline{w}}{\partial z}+\frac{1}{r}\frac{\partial(\overline{\rho u'w'r})}{\partial r}=-\rho g \tag{5}$$

The integration of Eq. 5 on both mixing layers using Eq. 4 gives two relations linking the thicknesses of mixing layers to radial positions of mixing layers. The integration of Eq. 5 multiplied by $\overline{w}$ using Eq. 4 gives two other relations linking the thicknesses of mixing layers and radial positions of mixing layers to a component of the Reynolds' shearing stress tensor.

Simple mixing length expressions proposed by Prandtl and Taylor can be used for this component (Eq. 6 ; Abramovich, 1963) :

$$\overline{u'w'}=-c_T z^2 \left|\frac{\partial \overline{w}}{\partial r}\right| \frac{\partial \overline{w}}{\partial r} \qquad (6)$$

For Prandtl's mixing length model (Eq. 7a) :

$$c_T=0.5 a_T^3 \qquad (7a)$$

For Taylor's mixing length model (Eq. 7b) :

$$c_T=a_T^3 \qquad (7b)$$

with $a_T = 0.09$

For each axial distance z, four coupled equations linking thicknesses of layers and lower radial limits of layers are obtained (Appendix A). They involve characteristics of mixing layers for lower axial distances. Theoretical radial limits of both layers as a function of axial distance z can be deduced from this system if initial conditions are known. We assumed zero initial thicknesses for z=0.

3.2. Comparison of experimental and theoretical results

Theoretical limits of shear layers according to Abramovich's model and Viswanathan's models are presented on Fig. 5 to Fig. 8 in order to compare experimental and theoretical secondary core's lengths. From axial temperature measurements, lengths of secondary cores seem higher for argon/helium jets than for air/air jets. For given densities, lengths are higher for $W_1/W_2=0.5$ than for $W_1/W_2=2$.

Both for air/air jets and for argon/helium jets, theoretical results seem to under-estimate the spreading rates of mixing layers for $W_1/W_2=0.5$ and $W_1/W_2=2$, maybe because drag

phenomena are not taken into account. The lengths of potential cores are therefore over-estimated. Theoretical results indicate that the length of the secondary core is higher for W_1=20 m.s^{-1} and W_2=40 m.s^{-1} than for W_1=40 m.s^{-1} and W_2=20 m.s^{-1}, which is in agreement with experimental results.

According to radial temperature measurements, the development of the inner mixing layer for argon/helium jets seems particularly under-evaluated by Abramovich's model (Fig. 9). As a consequence, the model based on local equations -with Taylor's mixing length- has been used for following global model.

4. Experimental particle size distributions

Experimental PSD have been obtained from in situ light-scattering measurements, for $SnCl_4/H_2O$ jets of various velocities, nozzle shape, densities and partial pressures.

4.1. Influence of velocities

The influence of both velocities W_1 and W_2 on mean diameters of PSD2 are shown on Fig. 10. The global tendency is an increase of mean diameters when velocities decrease. The influence of W_1 is high compared to that of W_2. As a consequence, W_1 is a parameter more appropriate than parameters based on shear, like $\ln(W_2/W_1)$. Shear between gases is however known to influence macromixing in the near-field of the jet.

4.2. Influence of nozzle shape

In order to study the consequences of nozzle shape on final PSD, powder has been produced with four different nozzles.

PSD obtained with two different double coaxial nozzles are compared on Fig. 11. One of the nozzles is made of tubes with a thickness of 1.0 mm (nozzle 1). The other one has been worked out in order to obtain walls with a thickness of 0.2 mm (nozzle 2). This parameter has been studied because the wall thickness may have an influence on macromixing in the near-field of the nozzle. Results show little differences for a given value of W_1, W_2 being kept equal to 20 $m.s^{-1}$.

PSD obtained with a double coaxial nozzle (nozzle 1) and a triple coaxial nozzle (nozzle 3) are compared on Fig. 12 and Fig. 13. The intermediate annular flow of nitrogen may also affect macromixing in the near-field of the nozzle. Results show few differences for a given set of velocities, the exit velocity of the intermediate flow being kept equal to 34 $m.s^{-1}$.

A comparison of mean diameters for two triple coaxial nozzles of thickness 0.2 mm (nozzle 4) and 1.0 mm (nozzle 3) also shows little variations for a given set of velocities (Fig. 14).

The use of two different velocities for the intermediate jet of nitrogen with nozzle 3 (12 $m.s^{-1}$ and 34 $m.s^{-1}$) does not lead to a significant change in mean diameters.

To conclude, nozzle shape seems to have little effect on particle formation for this $SnCl_4/H_2O$ system.

4.3. Influence of densities

Fig. 15 shows the influence of densities of carrier gases on mean diameters. Experimental and theoretical results of section 3 indicate a noticeable change in the development of mixing layers so that a strong influence on final PSD was expected. In fact, the use of two gases of different densities as carrier gases changes moderately final PSD. A general

increase of mean diameters is obtained with $SnCl_4(Ar)/H_2O(He)$ jets. It probably results from lower momentum fluxes increasing agglomeration in the container.

4.4. Influence of partial pressures of reagents

Fig. 16 presents mean diameters of PSD2 as a function of $\ln(W_2/W_1)$ for $SnCl_4(N_2)/H_2O(N_2)$ double jets. For given velocities W_1 and W_2 and in the range of our experiments, final mean diameters increase when partial pressures of reagents increase.

Interesting considerations can be obtained from following jets, with nozzle 1 :

jet 1 : Pp1=Pp2=7.1 kPa ; W_1=10 m.s^{-1} ; W_2=40 m.s^{-1}

jet 2 : Pp1=Pp2=3.5 kPa ; W_1=20 m.s^{-1} ; W_2=40 m.s^{-1}

Characteristics of the flow in the principal region of the jet are roughly the same for jet 1 and jet 2 (ratio of momentum fluxes 0.95). Global flux of $SnCl_4$ is also the same, so that the volume fraction of solid in the principal region, for a constant composition, is also approximately the same. However, experimental mean diameter for PSD2 is about 0.48 µm for jet 1 whereas it is only 0.32 µm for jet 2.

5. Discussion

5.1. Modelling of mixing and agglomeration

The model has been presented in Ablitzer et al. (2001).

Description of the development of inner and outer shear layers is obtained from Eq. 4, Eq. 5, Eq. 6 and Eq. 7b (Ablitzer, 1999). The computation of the model gives the theoretical development of inner and outer mixing layers in a gaseous double coaxial jet, for given exit velocities and densities. Quantities of reagents in mixing layers at abscissa z are deduced from calculated

limits and global conservation equations for mass and momentum, integrated between nozzle exit (z=0) and abscissa z.

The spread of the jet in the principal region is deduced from Abramovich (1963). Theoretical jets are vertical and develop downwards. As exit temperatures of gases are higher than the atmospheric temperature, the momentum of the jet is not conserved so that jets have finite lengths, depending on initial momentum. The decrease of momentum in the jet is evaluated numerically, step by step, as a function of densities effects.

Mesomixing has been taken into account according to Corrsin (1964). Reaction and nucleation are supposed instantaneous. Particles have been supposed to grow only by agglomeration, with instantaneous coalescence.

Agglomeration can be described by means of a population balance equation in its discrete form. (Eq. 8 and Eq. 9) :

$$i>1 \quad V_{agglo,i}=\frac{1}{2}\sum_{j=1}^{i-1}K_{(i-j),j}n_j n_{(i-j)}-\sum_{j=1}^{\infty}K_{ij}n_i n_j \qquad (8)$$

$$i=1 \quad V_{agglo,1}=B-\sum_{j=1}^{\infty}K_{1j}n_1 n_j \qquad (9)$$

$V_{agglo,i}$ is the rate of creation of particles in class i. B is a source term accounting for nucleation. K_{ij} is the agglomeration kernel for particles in classes i and j. n_i is the number density of particles in class i.

The agglomeration kernels are expressed as the sum of Brownian and turbulent contributions (Eq. 10) :

$$K_{ij} = (K_{ij})Br + (K_{ij})turb \qquad (10)$$

Brownian kernels depend on Knudsen number Kn (mean free path ℓ of the molecules in the gaseous surrounding divided by the size of the particle) (Hidy, 1969).

In the free molecule regime, corresponding approximately to Kn>5, agglomeration kernels are (Eq. 11) :

$$(K_{ij})_{Br}=(r_i+r_j)^2\left[8\pi kT\left(\frac{1}{m_i}+\frac{1}{m_j}\right)\right]^{\frac{1}{2}} \tag{11}$$

where r_i is the mean radius of particles in class i, k is Boltzmann's constant and m_i is the mean mass of particles in class i.

In the continuum regime, corresponding approximately to Kn<5, agglomeration kernels are given by Eq. 12 and Eq. 13 :

$$(K_{ij})_{Br} = 4\pi\,(r_i+r_j)\,(D_i+D_j) \tag{12}$$

$$D_i=\frac{kT}{6\pi\mu r_i}\left(1+\frac{\ell}{r_i}\left(1.257+0.400\exp(-1.10 r_i/\ell)\right)\right) \tag{13}$$

where μ is the dynamic viscosity of the surrounding gas.

The turbulent kernel is evaluated according to (Eq. 14) (Smoluchowski, 1917 ; Camp & Stein, 1943) :

$$(K_{ij})_{turb}=1{,}33\sqrt{\frac{\varepsilon}{\nu}}\left(r_i+r_j\right)^3 \tag{14}$$

where ε is the dissipation rate of turbulent energy per unit mass and ν is the kinematic viscosity of the gaseous surrounding.

Theoretical PSD (PSD1 and PSD2) obtained with this simple model based on agglomeration are not in agreement with experimental results (Fig. 17 and Fig. 18). Theoretical PSD appear noticeably influenced by the outer velocity W_2, whereas experimental PSD seem mainly influenced by the value of the inner velocity W_1, especially for PSD1.

5.2. Considerations about the improvement of previous model

Previous model has been used for $TiCl_4/H_2O$ jets and theoretical results have been compared to experimental PSD (Ablitzer et al., 2001). Satisfactory agreement has been obtained for this system. According to this model, particle growth resulted only from agglomeration, mainly in the principal region of the jet and in the container. The average volume calculated for a particle leaving the jet was about 30% to 55% of the average volume calculated for a particle in the container 15 s after the end of the jet. This satisfactory agreement may indicate that agglomeration was correctly represented. On the contrary, for $SnCl_4/H_2O$ jets, mean diameters are globally under-evaluated so that another growth phenomenon may be involved (Fig. 17 and 18). It is known that the reactivity of $SnCl_4$ is lower than the reactivity of $TiCl_4$. Partial hydrolysis may occur in the case of $SnCl_4$ and oxychlorides or hydroxychlorides may be formed. Because of the low reactivity, a surface growth involving $SnCl_4$ or one of these compounds is possible and could explain our experimental results. A high initial dispersion rate of $SnCl_4$ (i.e. high W_1) may be favourable to a fast and complete hydrolysis and so unfavourable to the additional growth phenomenon. On the contrary, a low dispersion rate (i.e. low W_1) may be favourable to partial reactions and so may stimulate the additional growth phenomenon.

Final PSD (PSD1 and PSD2) are moderately influenced by densities of gases, as shown on Fig. 15. In fact, the difference between mean diameters for $SnCl_4(N_2)/H_2O(N_2)$ and $SnCl_4(Ar)/H_2O(He)$ jets may be attributed to the characteristics of agglomeration in the container. The use of an intermediate jet of nitrogen and a change in the thickness of walls for $SnCl_4(N_2)/H_2O(N_2)$ jets do not have any noticeable influence on final PSD either. These operating conditions are assumed to have an influence on the development of mixing layers in the near-field of the jet, so that this aspect of mixing is probably not determining for final PSD, for the $SnCl_4/H_2O$ system and in our experimental conditions.

Experimental results seem strongly influenced by the value of the inner velocity W_1 (Fig. 10). As the outer gas generally represents a much higher volumetric flow rate than the inner gas (s_2/s_1=5.4 for nozzle 2), it is determining for the characteristics of the flow in the principal region of the jet. The influence of W_1 on the characteristics of the flow is thus noticeable only in the near-field of the jet. Considerations about the influence of partial pressures on PSD also indicate that global characteristics in the principal region of the jet are not determining.

We can assume from previous results that mesomixing involving the inner gas in the near-field of the jet may be determining for final PSD, probably because of a coupling with the additional growth phenomenon. So, the model for mesomixing should be improved in the near field in order to account for the influence of inner velocity W_1.

6. Conclusions

PSD resulting from $SnCl_4/H_2O$ reactive jets have been measured for various sets of velocities, nozzle shape, densities of carrier gas and partial pressures of reagents. A comparison of measurements with results of a simple model based on agglomeration shows that agglomeration is probably coupled to another growth phenomenon. It may involve $SnCl_4$ and probably occurs in the near-field of the jet. Further studies about this phenomenon would be of interest.

Final PSD do not seem to be influenced by the development of mixing layers between gases (macromixing) but rather by mesomixing near the nozzle exit. This probably results from a strong coupling of this aspect of mixing with the second growth phenomenon.

As a result of presented experiments, the inner velocity W_1 of the coaxial jet seems to be a major parameter for final PSD in the case of the $SnCl_4/H_2O$ system. This conclusion seems however highly dependent of properties of the reactive system.

Appendix A

An adimensional distance is introduced for the mixing layer between gas i and gas j :

$$\eta_{j(j+1)} = \frac{(r - r_j)}{b_{j(j+1)}}$$

Index 1 is used for the inner gas, index 2 for the outer gas and index 3 for the atmospheric gas.

$b_{j(j+1)}$ is the half velocity thickness of the mixing layer between gases i and j (layer j(j+1)) ; it is used for the characterisation of a layer when the velocity profile is assumed semi-infinite. We used the velocity profile proposed by Viswanathan & Morris (1992). r_j is the upper limit of the potential core j.

$\overline{w_{j(j+1)}}$ is the mean axial velocity in layer j(j+1) adimensioned with W_1 ; it is a function of $\eta_{j(j+1)}$.

$\overline{\rho_{j(j+1)}}$ is the mean density in layer j(j+1) adimensioned with ρ_1 ; it is a function of $\eta_{j(j+1)}$.

We define : $R_i=W_i/W_1$ and $S_i=\rho_i/\rho_1$.

c_{eq} is a coefficient linking the conventional finite thickness δ of a mixing layer with its half-velocity thickness b, according to $\delta=c_{eq}\, b$. We used $c_{eq}=2.58$ (Ablitzer, 1999).

As velocities are high in the near-field, the gravitation term is neglected in Eq. 4. The integration of Eq. 5 on both mixing layers using Eq. 4 gives two relations linking the thicknesses of mixing layers to radial positions of mixing layers.

- For inner mixing layer (between gases 1 and 2) :

$$(1 - R_2)(r_1^2 - 1) + 2\beta_{11}\, r_1 b_{12} + 2\beta_{12}\, b_{12}^2 = 0$$

with

$$\beta_{j1} = \int_0^{ceq} \overline{\rho_{j(j+1)}}\,\overline{w_{j(j+1)}}\,(\overline{w_{j(j+1)}} - R_{(j+1)})\, d\eta_{j(j+1)}$$

$$\beta_{j2} = \int_0^{ceq} \overline{\rho_{j(j+1)}}\,\overline{w_{j(j+1)}}\,(\overline{w_{j(j+1)}} - R_{(j+1)})\, \eta_{j(j+1)}\, d\eta_{j(j+1)}$$

- For outer mixing layer (between gases 2 and 3) :

$$(r_1^2 - 1) + 2\left(\beta_{14}\, b_{12}^2 + \frac{\beta_{22} b_{23}^2}{(R_2 - R_3)}\right) + 2\left(\beta_{13}\, r_1 b_{12} + \frac{\beta_{21} r_2 b_{23}}{(R_2 - R_3)}\right) + R_2 S_2 (r_2^2 - r_{02}^2 - (r_1 + c_{eq}\, b_{12})^2 + 1) = 0$$

with

$$\beta_{j3} = \int_0^{ceq} \overline{\rho_{j(j+1)}}\,\overline{w_{j(j+1)}}\, d\eta_{j(j+1)}$$

$$\beta_{j4} = \int_0^{ceq} \overline{\rho_{j(j+1)}}\,\overline{w_{j(j+1)}}\, \eta_{j(j+1)}\, d\eta_{j(j+1)}$$

The integration of Eq. 5 multiplied by $\overline{w}$ using Eq. 4 gives two other relations linking the thicknesses of mixing layers and radial positions of mixing layers to a component of the Reynolds' shearing stress tensor.

- For inner mixing layer :

$$(1-R_2{}^2)\frac{d(r_1{}^2)}{dz} + 2\beta_{15}\frac{d(r_1 b_{12})}{dz} + 2\beta_{16}\frac{d(b_{12}{}^2)}{dz} = 4\int_0^{ceq} \overline{\rho_{12}}\,\overline{u'_{12}\,w'_{12}}(b_{12}\eta_{12} + r_1)\frac{d(\overline{w_{12}})}{d\eta_{12}} d\eta_{12}$$

- For outer mixing layer :

$$\frac{d(r_1)^2}{dz} + S_2 R_2\left(\frac{d(r_2{}^2)}{dz} - \frac{d(r_1 + c_{eq}\, b_{12})^2}{dz}\right) + \frac{2\beta_{26}}{(R_2{}^2 - R_3{}^2)}\frac{d(b_{23}{}^2)}{dz} + 2\beta_{14}\frac{d(b_{12}{}^2)}{dz} + 2\beta_{13}\frac{d(r_1 b_{12})}{dz}$$

$$+\frac{2\beta_{25}}{(R_2{}^2 - R_3{}^2)}\frac{d(r_2 b_{23})}{dz} = \frac{4}{(R_2{}^2 - R_3{}^2)}\int_0^{ceq} \overline{\rho_{23}}\,\overline{u'_{23}\,w'_{23}}(b_{23}\eta_{23} + r_2)\frac{d(\overline{w_{23}})}{d\eta_{23}} d\eta_{23}$$

with

$$\beta_{j5} = \int_0^{ceq} \overline{\rho_{j(j+1)}}\,\overline{w_{j(j+1)}}\,(\overline{w_{j(j+1)}}^2 - R_{(j+1)}{}^2)\, d\eta_{j(j+1)}$$

$$\beta_{j6} = \int_0^{ceq} \overline{\rho_{j(j+1)}}\,\overline{w_{j(j+1)}}\,(\overline{w_{j(j+1)}}^2 - R_{(j+1)}{}^2)\, \eta_{j(j+1)}\, d\eta_{j(j+1)}$$

Notation

Symbols

B	nucleation rate, $m^{-3}.s^{-1}$
d	diameter, m
dp	mean diameter, m
I	light intensity with particles, $W.m^{-2}$
I_0	light intensity without particle, $W.m^{-2}$
k	Boltzmann's constant, $J.K^{-1}$
K_{ij}	agglomeration kernel for particles in classes i and j, $m^3.s^{-1}$
Kn	Knudsen number
ℓ	mean free path, m
L	optical path through the suspension, m
m_i	mean mass of particles in class i, kg
n_i	number density of particles in class i
Ppi	exit partial pressure of reagent in gas i, Pa
Pp	mean exit partial pressure, Pa
r_i	mean radius of particles in class i, m
s_i	exit section for gas i, m^2
T	mean temperature, K
T_i	mean exit temperature for gas i, K
W	mean velocity, $m.s^{-1}$
W_c	characteristic velocity, $m.s^{-1}$
W_i	mean exit velocity for gas i, $m.s^{-1}$
δ	finite thickness of a mixing layer, m
ε	dissipation rate of turbulent energy per unit mass, $m^2.s^{-3}$
λ	wavelength, m
μ	dynamic viscosity of the gaseous surrounding, Pa.s
ν	kinematic viscosity of the gaseous surrounding, $m^2.s^{-1}$
ρ	density, $kg.m^{-3}$
τ	turbidity, m^{-1}
(r,θ,z)	cylindrical co-ordinates
(u,v,w)	components of velocity

Subscripts

1	inner gas

2	outer gas

Abbreviations

PSD	Particle Size Distribution
PSD1	Particle Size Distribution for firstly measured particles
PSD2	Particle Size Distribution for particles 15s after the end of the jet
SEM	Scanning Electron Microscopy

References

Ablitzer, C., 1999, Etude de la formation de poudre dans des jets coaxiaux réactifs, *Ph. D. Thesis, INPG-ENSMSE, France* (in french)

Ablitzer, C., Gruy, F., & Perrais, C., 2001, Powder formation by hydrolysis of metallic chlorides in a coaxial gas jet - Experiments and modelling, *Chemical Engineering Science*, 56, 2409-2420

Abramovich, G.N., 1963, The theory of turbulent jets, *Ed. L.H. Schindel, The MIT Press*

Au, H., & Ko, N.W.M., 1987, Coaxial jets of different mean velocity ratios, Part 2, *Journal of Sound and Vibration*, 116 (3), 427-443

Brown, G.L., & Roshko, A., 1974, On density effects and large structure in turbulent mixing layers, *J. Fluid Mech.*, 64 (part 4), 775-816

Buresti, G., Petagna, P., & Talamelli, A., 1998, Experimental investigation on the turbulent near-field of coaxial jets, *Experimental Thermal and Fluid Science*, 17, 18-26

Buresti, G., Talamelli, A., & Petagna, P., 1994, Experimental characterization of the velocity field of a coaxial jet configuration, *Experimental Thermal and Fluid Science*, 9, 135-146

Camp, T.R., & Stein, P.C., 1943, *Boston Society of Civil Engineers*, 30, 219

Champagne, F.H., & Wygnanski, I.J., 1971, An experimental investigation of coaxial turbulent jets, *Int. J. Heat Transfer.*, 14, 1445-1464, 1971

Corrsin, S., 1964, The isotropic Turbulent Mixer : Part II Arbitrary Schmidt Number, *AIChE J.*, 10 (6), 870-877

Dahm, W.J.A., Frieler, C.E., & Tryggvason, G., 1992, Vortex structure and dynamics in the near field of a coaxial jet, *J. Fluid Mech.*, 241, 371-402

Delattre, P., & Friedlander, S.K., 1978, Aerosol coagulation and diffusion in a turbulent jet, *Ind. Eng. Chem. Fundam.*, 17(3), 189-194

Dimotakis, P.E., 1986, Two dimensional shear-layer entrainment, *AIAA Journal*, 24 (11), 1791-1796

Durao, D., & Whitelaw, J.H., 1973, Turbulent mixing in the developing region of coaxial jets, *Journal of Fluids Engineering*, 467-473

Favre-Marinet, M., Camano, E.B., & Sarboch, J., 1999, Near-field of coaxial jets with large density differences, *Experiments in Fluids*, 26, 97-106

Habib, M.A., & Whitelaw, J.H., 1979, Velocity characteristics of a confined coaxial jet, *Journal of Fluids Engineering*, 101, 521-529

Hidy, G., 1969, "Aerosols" in "Surface and Colloid Science", vol 2, *Ed. E. Matijevic, Wiley Interscience*

Ko, N.W.M., & Au, H., 1985, Coaxial jets of different mean velocity ratios, *Journal of Sound and Vibration*, 100 (2), 211-232

Ko, N.W.M., & Kwan, S.H., 1976, The initial region of subsonic coaxial jets, *J. Fluid Mech.*, 73 (part 2), 305-332

Koch, W., Windt, H., & Karfich, N., 1993, Modeling and experimental evaluation of an aerosol generator for very high number currents based on a free turbulent jet, *J. Aerosol Sci.*, 24 (7), 909-918

Lesniewski, T., 1997, Particle nucleation and growth in turbulent jets, *Ph. D. Thesis, University of California*

Pratsinis, S.E., & Vemury, S., 1996, Particle formation in gases : a review, *Powder Technol.*, 88: 267-273

Saint-Raymond, H., Gruy, F., & Cournil, M., 1998, Turbulent aggregation of alumina in water and n-heptane, *J. Colloid Interface Sci.*, 202, 238-250

Smoluchowski, M., 1917, Versuch einer mathematischen Theorie der Koagulationskinetik Kolloider Lösungen, *Z. Physik. Chem.*, 92, 129-166

Viswanathan, K., & Morris, P.J., 1992, Predictions of turbulent mixing in axisymetric compressible shear layers, *AIAA Journal*, 30 (6), 1529-1536

List of figures

Fig. 1 Experimental set-up

Fig. 2 Principle of temperature measurements

Fig. 3 SEM observation of particles

Fig. 4 Probe for light-scattering measurements

Fig. 5 Macromixing in an air/air double jet for W_1=20 m.s^{-1} and W_2=40 m.s^{-1}

Fig. 6 Macromixing in an argon/helium double jet for W_1=20 m.s^{-1} and W_2=40 m.s^{-1}

Fig. 7 Macromixing in an air/air double jet for W_1=40 m.s^{-1} and W_2=20 m.s^{-1}

Fig. 8 Macromixing in an argon/helium double jet for W_1=40 m.s^{-1} and W_2=20 m.s^{-1}

Fig. 9 Macromixing in an argon/helium double jet for W_1=40 m.s^{-1} and W_2=30 m.s^{-1}

Fig. 10 $SnCl_4/H_2O$ double jets : Influence of velocities on PSD2

Fig. 11 $SnCl_4/H_2O$ double jets : Influence of nozzle thickness on PSD2

Fig. 12 $SnCl_4/H_2O$ jets : Influence of a third annular jet on PSD2

Fig. 13 $SnCl_4/H_2O$ jets : Influence of a third annular jet on PSD1

Fig. 14 $SnCl_4/H_2O$ triple jets : Influence of the nozzle thickness on PSD1

Fig. 15 $SnCl_4/H_2O$ double jets : Influence of densities of gases on PSD2

Fig. 16 $SnCl_4/H_2O$ double jets : Influence of partial pressures of reagents on PSD2

Fig. 17 $SnCl_4/H_2O$ double jets : Experimental and theoretical results for PSD2

Fig. 18 $SnCl_4/H_2O$ double jets : Experimental and theoretical results for PSD1

List of tables

Tab. 1 Characteristics of nozzles

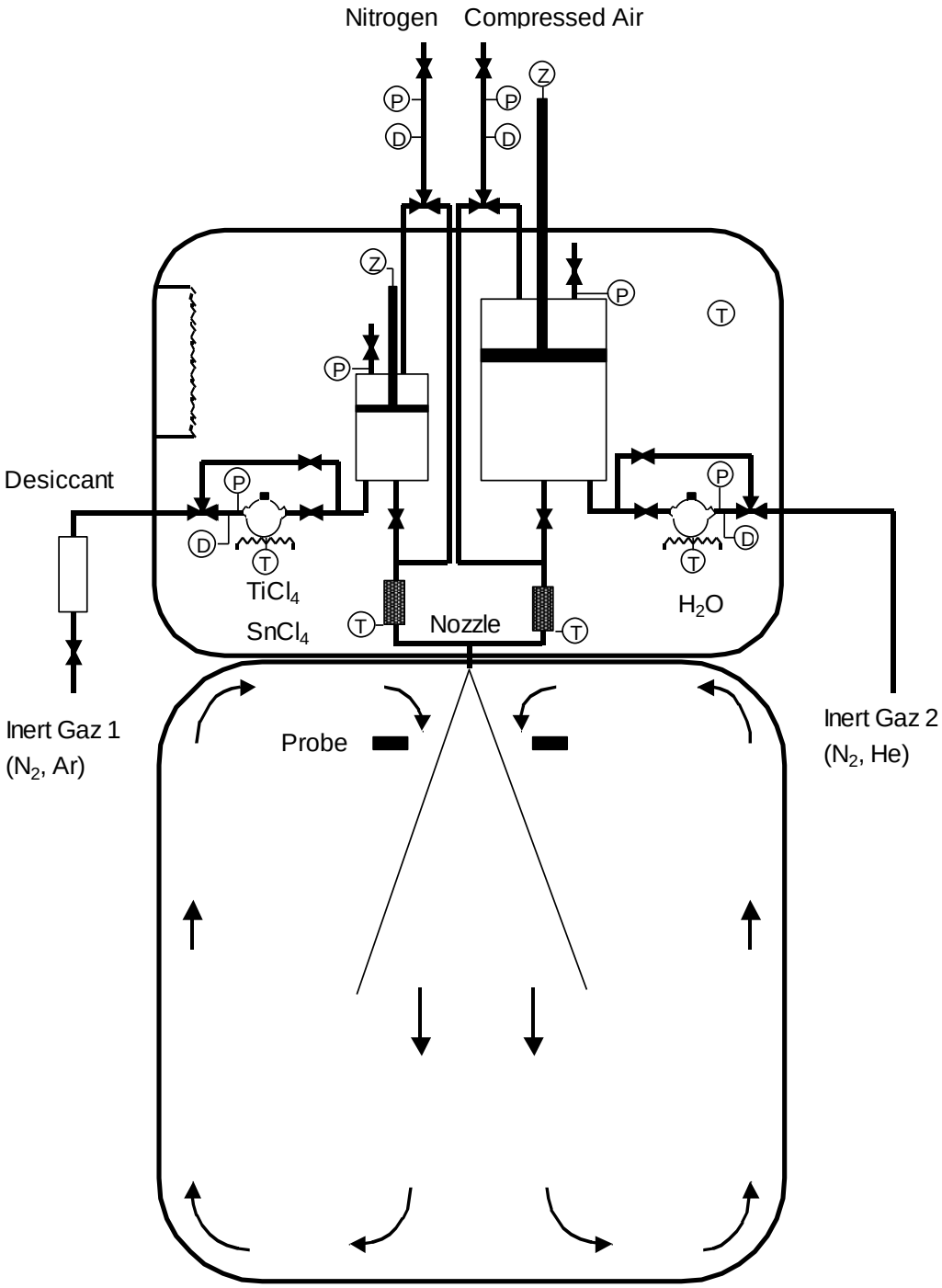

Fig. 1 : Experimental set-up

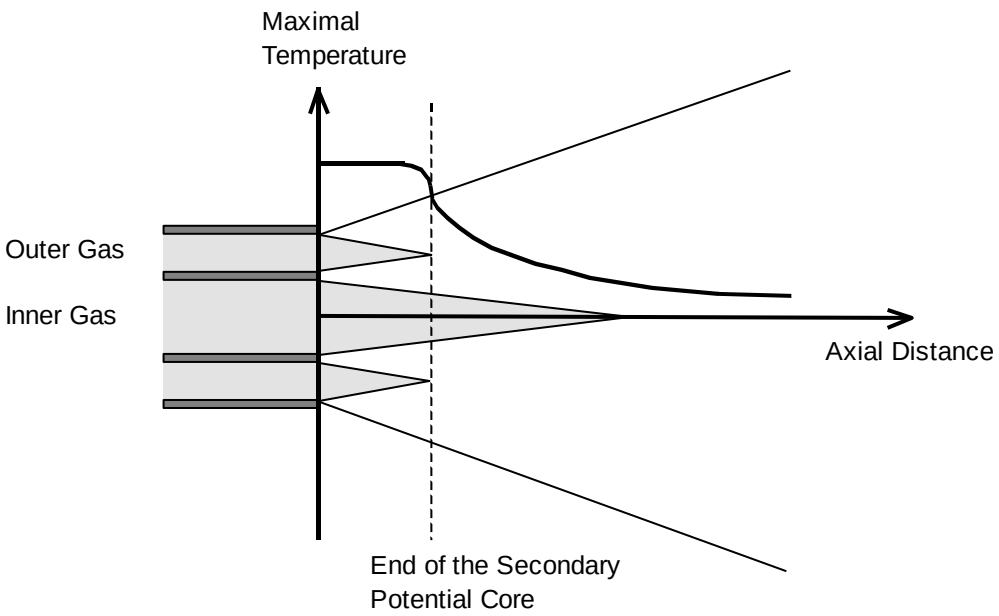

Fig. 2 : Principle of temperature measurements

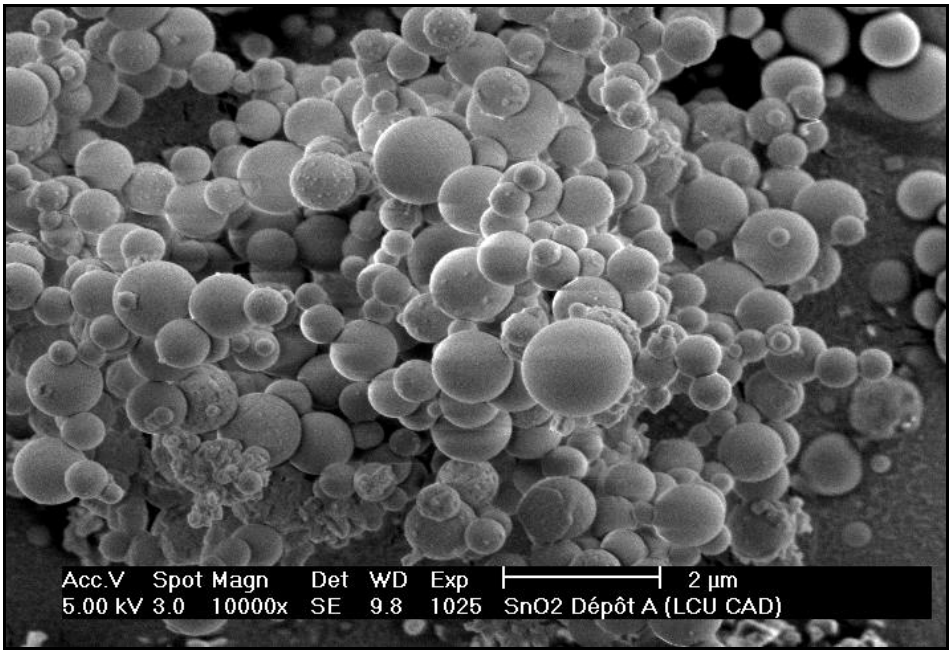

Fig. 3 : SEM observation of particles

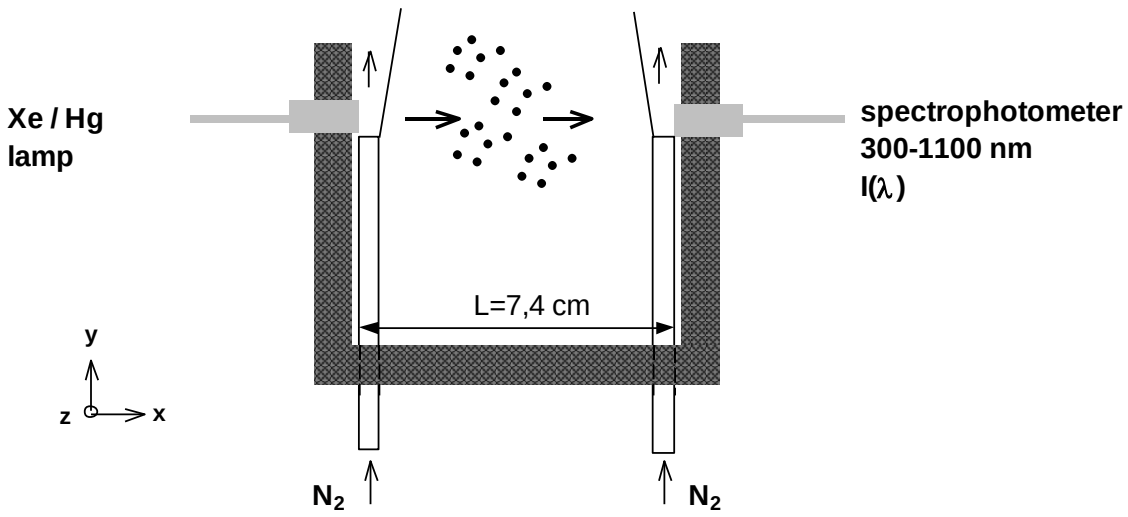

Fig. 4 : Probe for light-scattering measurements

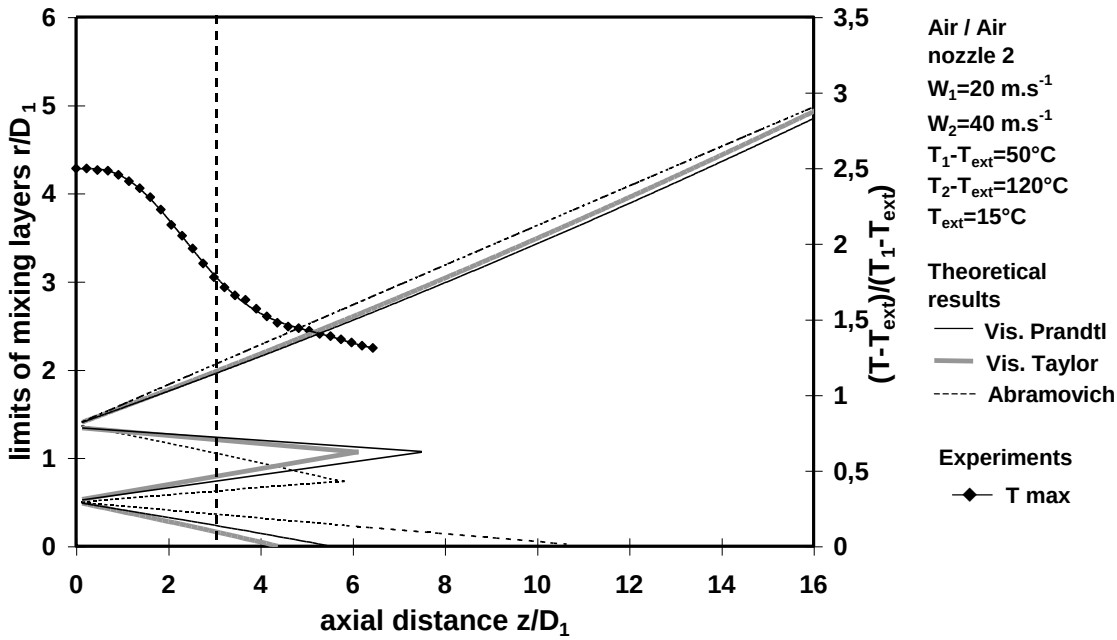

Fig. 5 : Macromixing in an air/air double jet for W_1=20 m.s^{-1} and W_2=40 m.s^{-1}

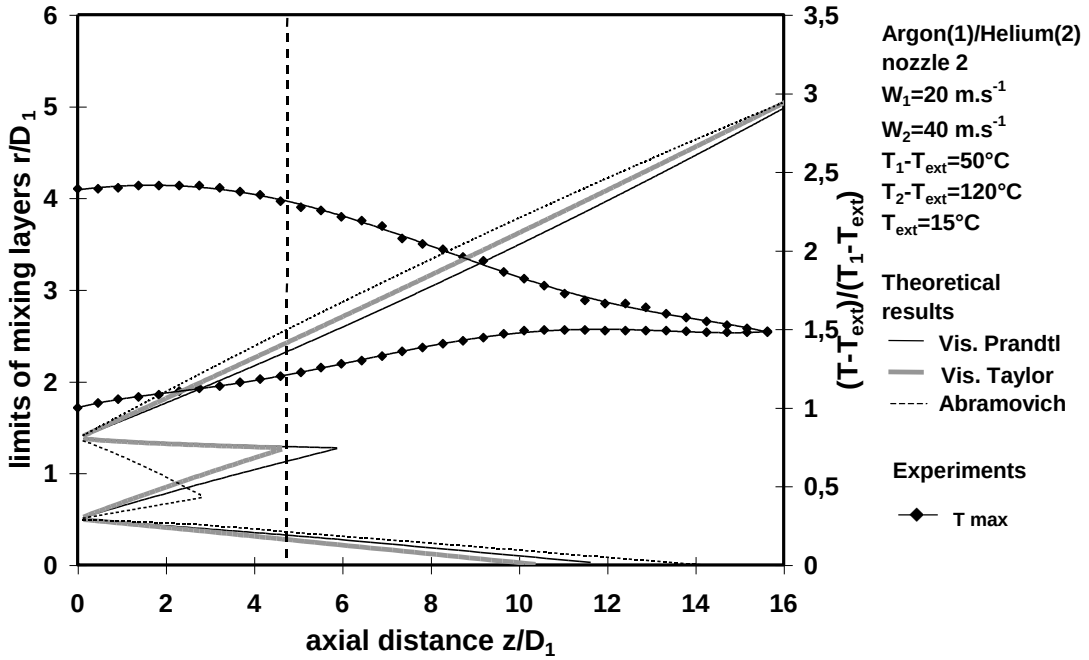

Fig. 6 : Macromixing in an argon/helium double jet for W_1=20 m.s^{-1} and W_2=40 m.s^{-1}

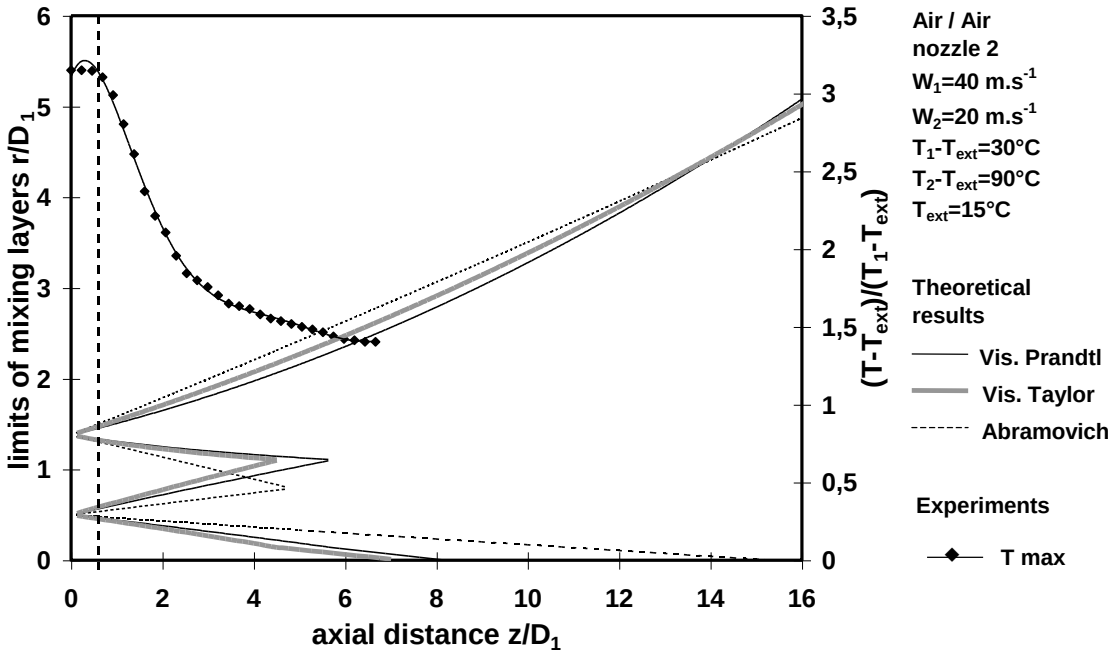

Fig. 7 : Macromixing in an air/air double jet for W_1=40 m.s^{-1} and W_2=20 m.s^{-1}

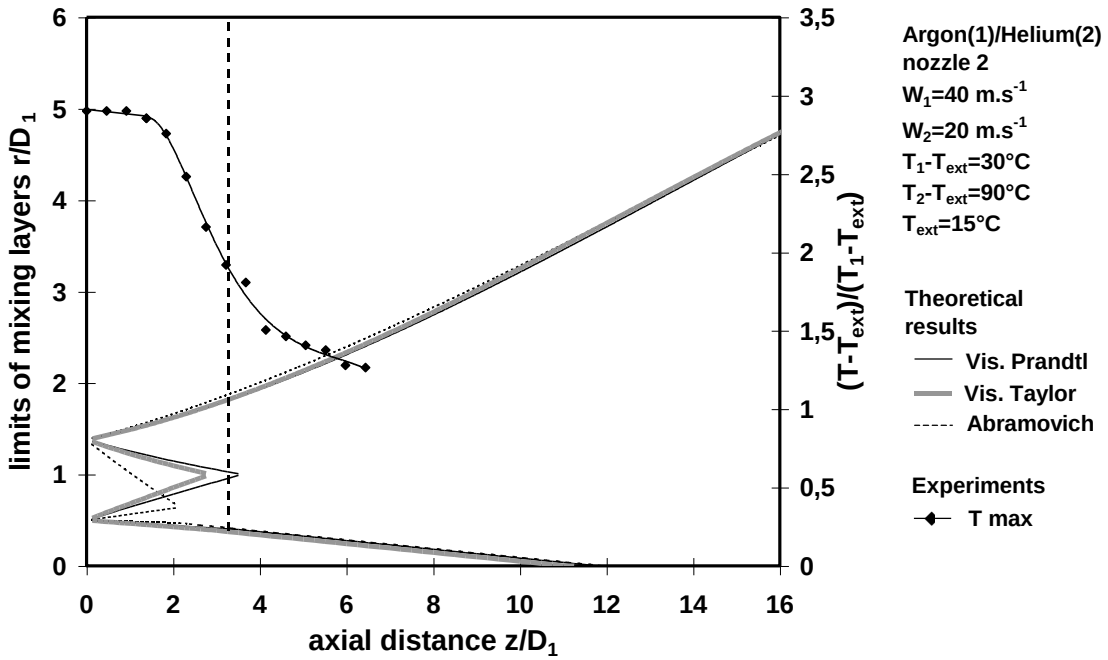

Fig. 8 : Macromixing in an argon/helium double jet for W_1=40 m.s^{-1} and W_2=20 m.s^{-1}

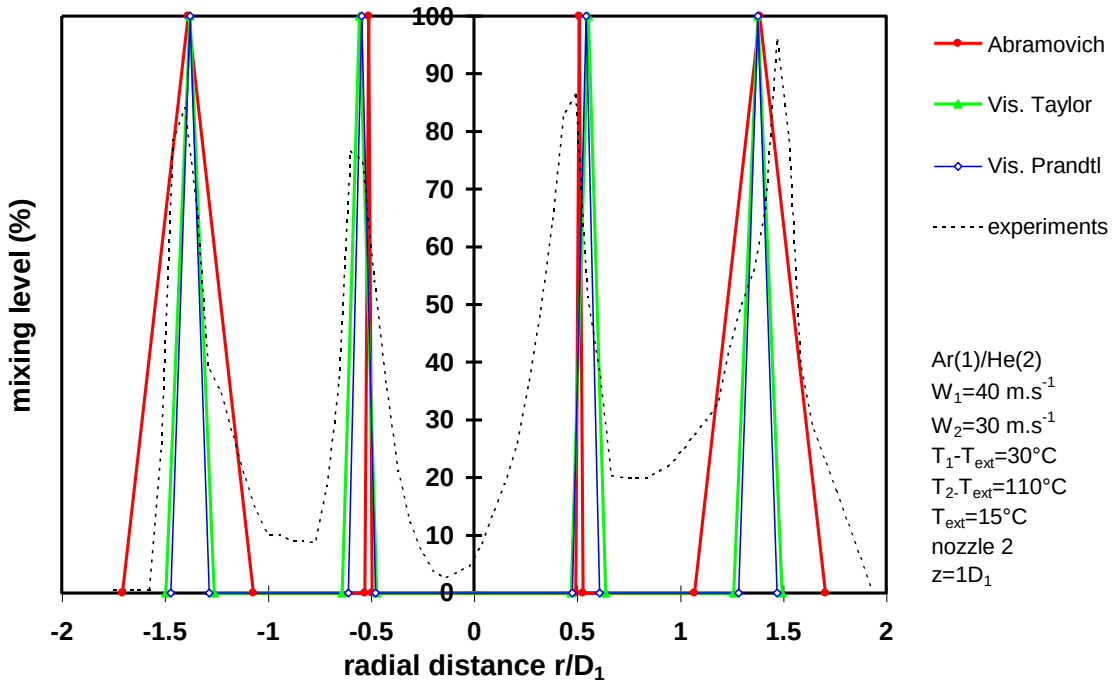

Fig. 9 : Macromixing in an argon/helium double jet for W_1=40 m.s^{-1} and W_2=30 m.s^{-1}

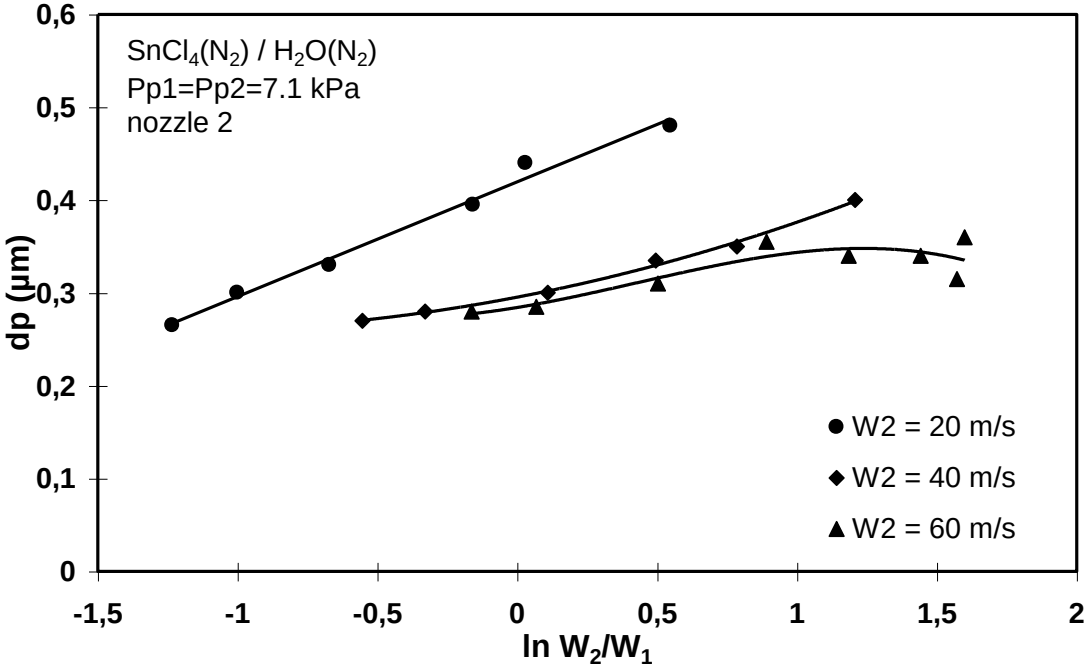

Fig. 10 : $SnCl_4/H_2O$ double jets
Influence of velocities on PSD2

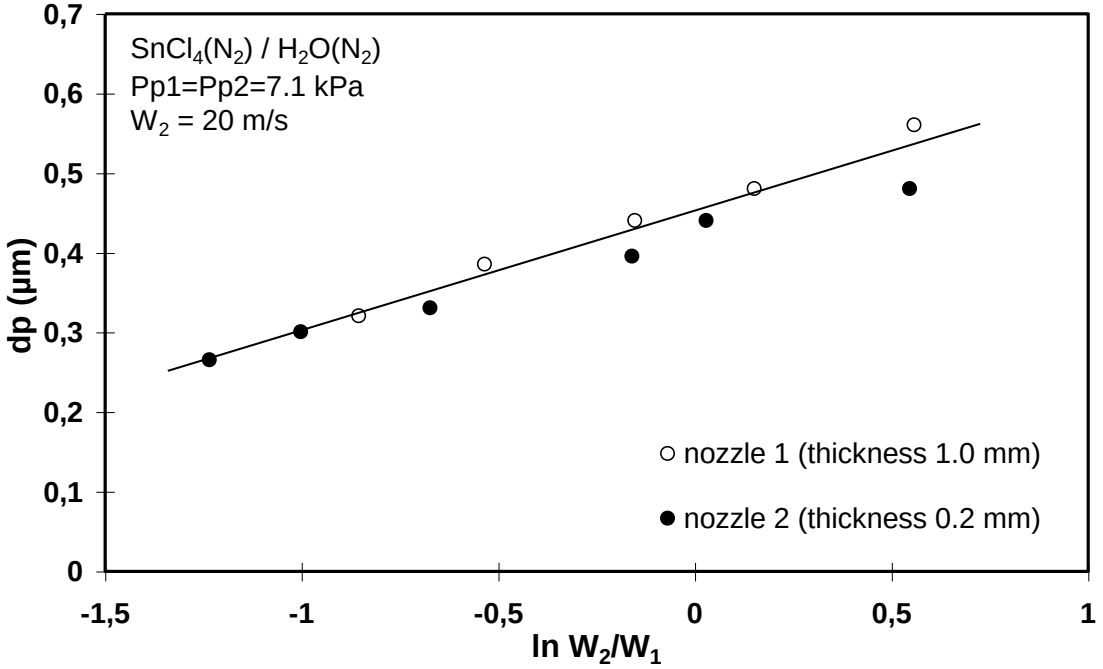

Fig. 11 : $SnCl_4/H_2O$ double jets
Influence of nozzle thickness on PSD2

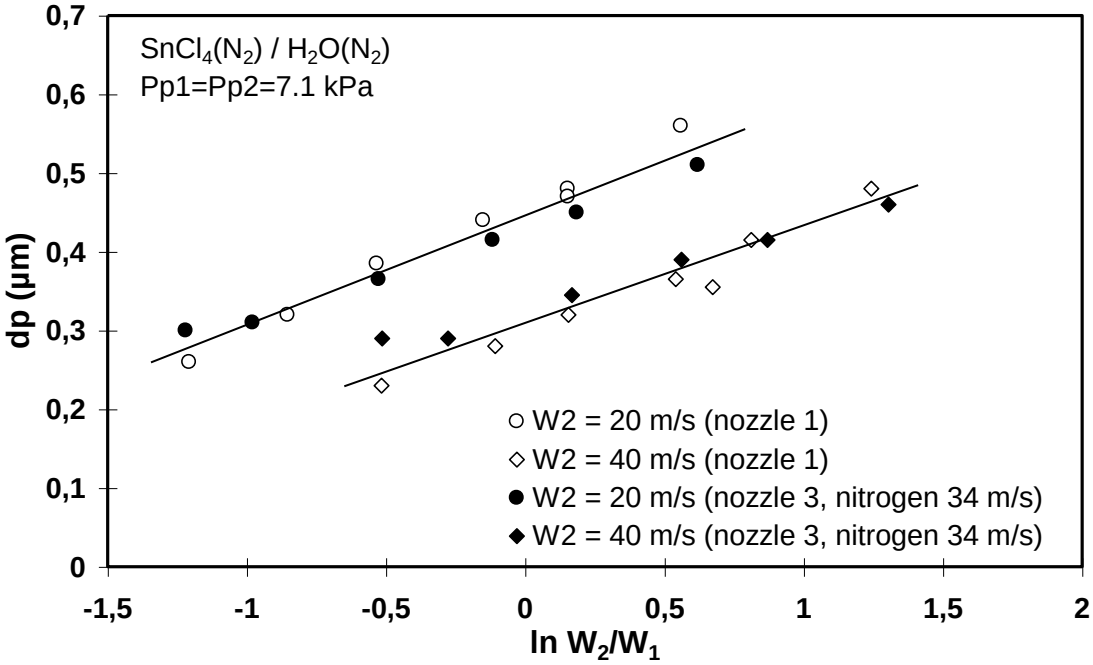

Fig. 12 : $SnCl_4/H_2O$ jets
Influence of a third annular jet on PSD2

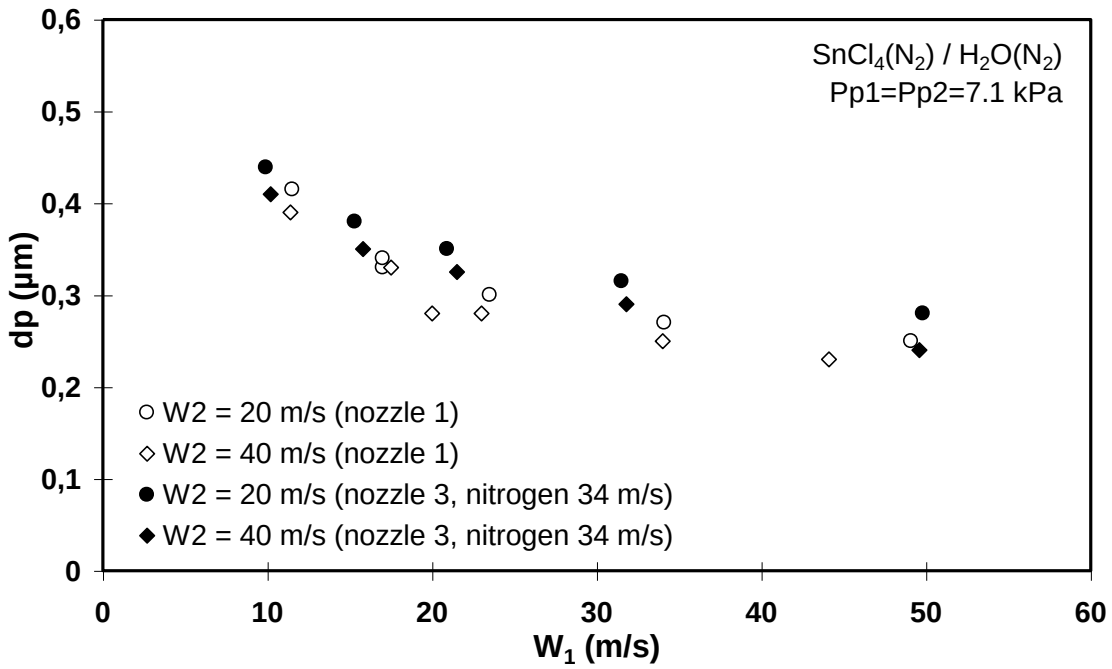

Fig. 13 : $SnCl_4/H_2O$ jets
Influence of a third annular jet on PSD1

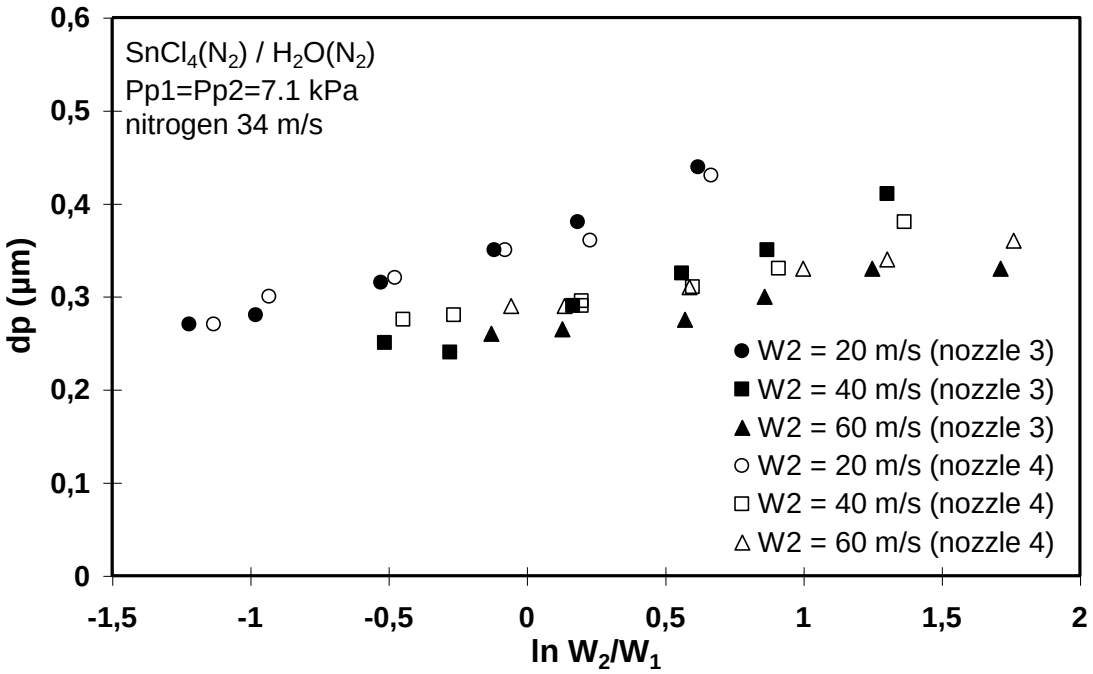

Fig. 14 : $SnCl_4/H_2O$ triple jets
Influence of the nozzle thickness on PSD1

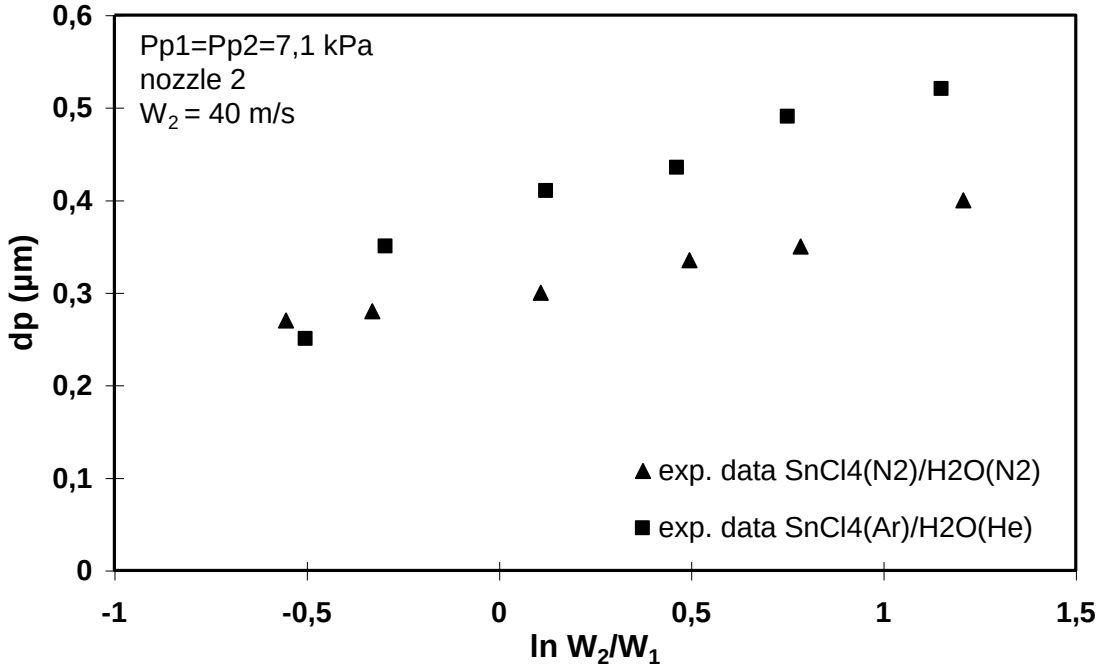

Fig. 15 : $SnCl_4/H_2O$ double jets
Influence of densities of gases on PSD2

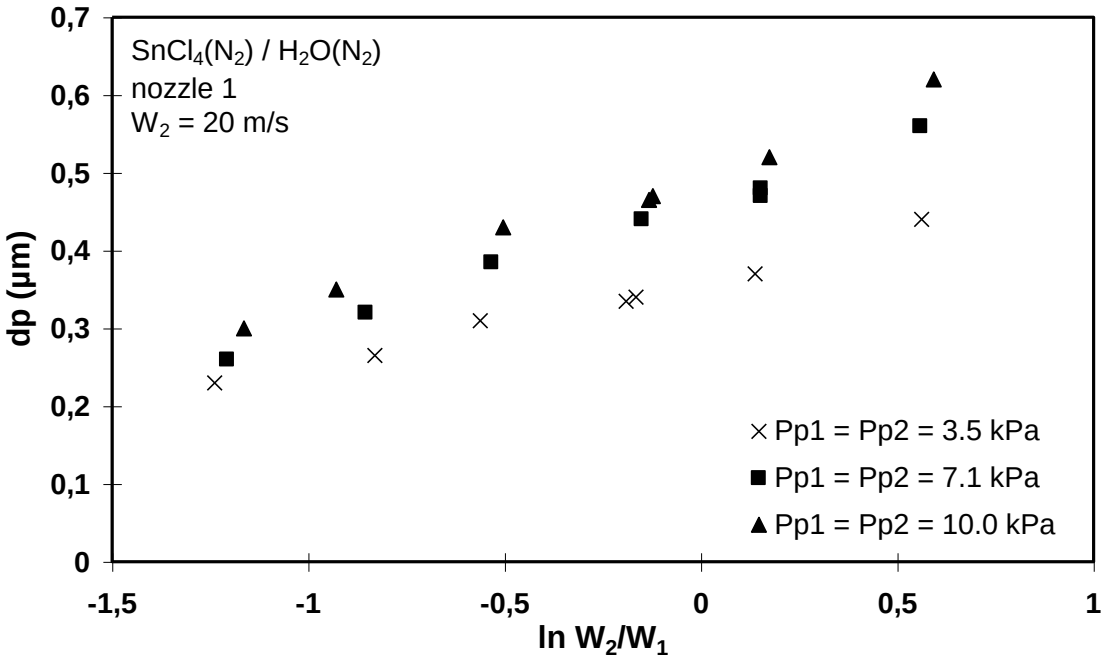

Fig. 16 : $SnCl_4/H_2O$ double jets
Influence of partial pressures of reagents on PSD2

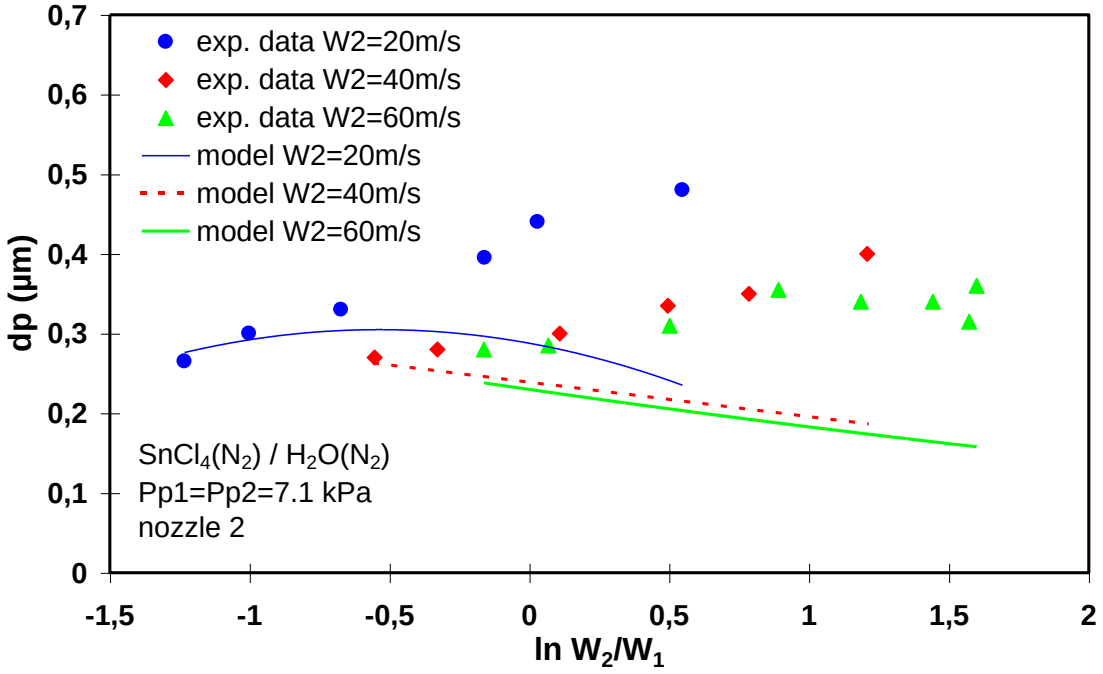

Fig. 17 : $SnCl_4/H_2O$ double jets
Experimental and theoretical results for PSD2

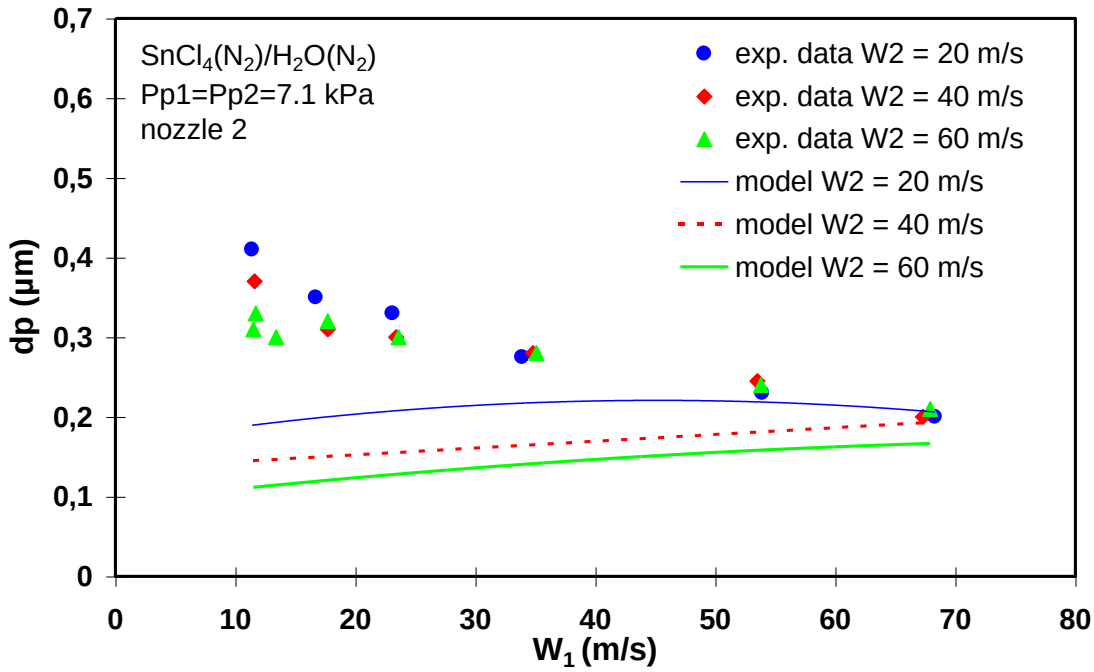

Fig. 18 : $SnCl_4/H_2O$ double jets
Experimental and theoretical results for PSD1

nozzle	nozzle 1	nozzle 2	nozzle 3	nozzle 4
inner diam. inner tube (mm)	4.35	4.35	4.35	4.35
inner diam. intermediate tube (mm)	none	none	8.0	8.0
inner diam. outer tube (mm)	12.0	12.0	14.0	14.0
thickness of tubes (mm)	1.0	0.2	1.0	0.2

Table 1 : Characteristics of nozzles